Statistics of 'worms' in Penrose tilings



1989 J. Phys. A: Math. Gen. 22 4347

(http://iopscience.iop.org/0305-4470/22/20/014)

J. Phys. A: Math. Gen. **22** (1989) 4347-4373. Printed in the UK

# Statistics of 'worms' in Penrose tilings

Andréi Pavlovitch†, Yuval Gefen‡ and Maurice Kléman§

† Section de Recherches de Métallurgie Physique (SRMP), Centre d'Etudes Nucléaires de Saclay, BP 2, 91191 Gif-sur-Yvette Cédex, France

‡ Department of Nuclear Physics, The Weizmann Institute of Science, Rehovot, 76100 Israel

§ Laboratoire de Physique des Solides (associé au CNRS), Bâtiment 510, Université de Paris-Sud, 91405 Orsay Cédex, France

Received 9 January 1989

**Abstract.** Certain structural aspects of two-dimensional Penrose tilings are studied using de Bruijn's pentagrid picture. We discuss the statistics of hexagons, decagons and 'worms' (sequences of adjacent hexagons bounded by two decagons). We show that within the discrete framework considered here, phason modes and structural transformation modes are located along particular 'worms' and we derive the spatial distribution of the latter.

**Résumé.** Certaines caractéristiques structurales des pavages de Penrose bidimensionnels sont étudiées dans le cadre de la pentagrille de de Bruijn. Nous calculons les statistiques des décagones, des hexagones et des 'tubes' (ce sont des séquences d'hexagones adjacents, bornées par deux décagones). Nous montrons que dans le cadre du modèle discret considéré ci-dessus, les modes de type 'phason' et 'transformation structurale' sont localisés suivant certains 'tubes', dont nous précisons la distribution spatiale.

## 1. Introduction

Future progress in the field of aperiodic crystals has to rely on detailed understanding of the structural properties of the latter. Much progress has been made in understanding the structure of infinite Penrose tilings (PT) (Penrose 1974, 1979, Gardner 1977, Grünbaum and Sheppard 1987) and analysing topological defects in such geometries (for a comprehensive overview of the subject see Gratias and Michel (1986) and Henley (1987)). The seminal work of de Bruijn (1981a, b) has demonstrated that a PT can be obtained by a direct projection of a five-dimensional hypercubic lattice onto a two-dimensional space. This method has been extended to quasicrystals in three dimensions as well (Kramer and Neri 1984, Duneau and Katz 1985). The relation between a high-dimensional periodic lattice and a lower-dimensional aperiodic lattice also enables us to define and classify topological defects in the latter (Levine *et al* 1985, Bak 1985, Kléman *et al* 1986, Bohsung and Trebin 1987).

The structure concerning *local scales* (as opposed to the hydrodynamical picture of quasicrystals) is not that well understood. Indeed, the statistics and hierarchical properties of PT, including finite domains in such structures, have been investigated (Gardner 1977, de Bruijn 1981a, b, Sadoc and Mosseri 1984) and expressed in terms of transfer matrices of fractals (Peyrière 1986, Gefen *et al* 1988). However, a detailed geometrical understanding of finite patterns and local (non-topological) defects in PT is still lacking. Such understanding appears to be necessary to determine the relevance of the theory of ideal quasicrystals to systems that occur in Nature. Whether such

0305-4470/89/204347+27$02.50  

systems are quasicrystals with imperfections or genuinely disordered systems is still an open question. It is simpler and therefore natural to consider as a first step two-dimensional PT.

An important issue in the present discussion is phason modes, first introduced by Levine *et al* (1985) and later shown to be related to local excitations (Kléman *et al* 1986, Socolar *et al* 1986). The analysis detailed below focuses on such local excitations and on the geometrical aspects of their propagation. For this purpose we employ the discrete model, put forward by de Bruijn (1981a, b). The relation between this discrete model and a hydrodynamic picture has been considered by Socolar *et al* (1986) and by Frenkel *et al* (1986).

Following a review of some important results of de Bruijn's analysis of PT, § 2 is devoted to a geometrical study of the strips of which a PT is made. These strips consist of sequences of rhombi adjacent along parallel edges. They may be considered as the natural 'substrates' for sequences of hexagons called 'worms' (Gardner 1977, de Bruijn 1981a, b, Socolar *et al* 1986) which, in turn, are the substrates of the local excitations discussed here. These worms are studied in § 3 where we present detailed statistics of their lengths and their elementary 'building blocks'. In § 4 we introduce phason excitations and structural transformations and investigate how they are manifested in terms of changes along worm configurations. We emphasise at this point that since the connection between atomic or molecular arrangements and quasicrystalline patterns is not yet completely understood, we shall not discuss here the energetics and dynamics associated with our structural defects. It is possible, of course, to assume certain dynamics for the propagation of phason excitations (hopping mechanism for example) but we shall not attempt at this point to relate our geometrical picture to measurable quantities.

## 2. Previous results, definitions and basic relations

In this section we shall define the ingredients of the geometry of worms. We first review some basic results pertaining to de Bruijn's picture, which will be employed subsequently in our analysis.

Figure 1($a$) shows a perfect two-dimensional PT. It consists of thin (t) and thick (T) arrowed rhombi (figure 1($b$)). These rhombi are put together to tile the plane and, at the same time, satisfy certain matching rules imposed by their arrowed edges. The PT of figure 1($a$) is the dual (up to continuous distortions) of a planar pentagrid shown in figure 2($a$). Figure 2($b$) depicts the intersections dual to the tiles ($t$) and ($T$) of figure 1($b$). The pentagrid consists of a superposition of five sets of parallel, equidistant lines perpendicular to the five directions $\boldsymbol{\nu}_j$ ($j = 0, \ldots, 4$) of a regular 5-star (figure 2($a$)). Any point $M$ belonging to the $j$th set of the pentagrid satisfies

$$\mathbf{OM} \cdot \boldsymbol{\nu}_j + \gamma_j = k_j \tag{2.1}$$

where $\mathbf{OM}$ is a planar vector corresponding to the point $M$ (O is an arbitrary origin). Here $k_j$ is an integer ($j$ labels the set; every point on a given line belonging to the set $j$, is described by the same $k_j$). $(\gamma_j)_{j=0,\ldots,4}$ is a set of five real numbers such that

$$\sum_{j=0}^{4} \gamma_j = C. \tag{2.2}$$

One gets the standard PT of figure 1($a$) if $C$ is an integer (de Bruijn 1981a, b). If $C$ is not an integer, the resulting generalised PT consists of four types of tiles T, t, T'

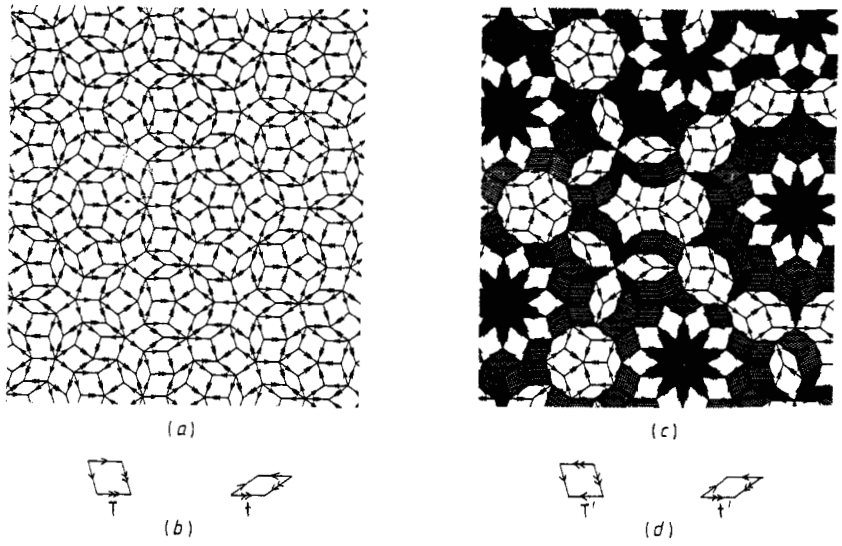


**Figure 1.** (*a*) A perfect Penrose tiling consisting of thin (t) and thick (T) rhombi (see de Bruijn 1981a, b). (*b*) The elementary rhombi (t) and (T) for the perfect Penrose tiling. (*c*) A generalised Penrose tiling ($\Sigma\ \gamma_j = 0, 5$) generated from t, T (white) and t', T' (dark) rhombi. (*d*) t' and T' rhombi (note the difference in the arrowing with t and T).

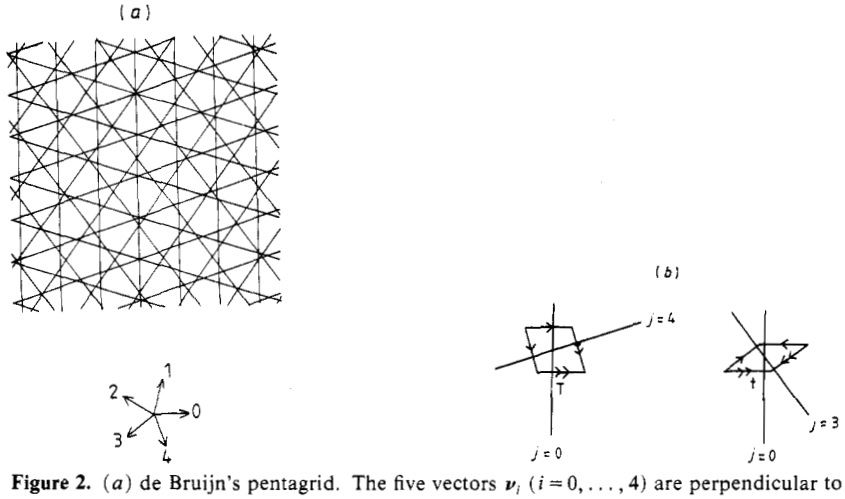


**Figure 2.** (*a*) de Bruijn's pentagrid. The five vectors $\boldsymbol{\nu}_i$ ($i = 0, \ldots, 4$) are perpendicular to the five sets of lines which make up the pentagrid. (*b*) Intersections of the pentagrid dual to the tiles (t) and (T) of figure 1(*b*).

and t' (figure 1(*c*, *d*)) (Pavlovitch and Kléman 1987). In this section and in § 3 we consider the geometry of worms on the standard PT only. We show in § 4 how generalised PT are obtained from the standard PT by introducing structural transformations along certain worms.

With each mesh of the pentagrid one can associate a set of five integers $(k_j)_{j=0,\ldots,4}$ defined by

$$k_j = \lceil \mathbf{OM} \cdot \boldsymbol{\nu} + \gamma_j \rceil \qquad (j = 0, \ldots, 4) \tag{2.3}$$

where $M$ is an arbitrary point of the mesh and $\lceil a \rceil$ denotes the smallest integer larger than $a$. Associated with each mesh is a unique set $(k_j)_{j=0,\ldots 4}$. De Bruijn has shown that (2.3) defines a subset of $Z^5$ such that the points

$$\mathbf{OP} = \sum_{j=0}^{4} k_j \boldsymbol{\nu}_j \tag{2.4}$$

are the vertices of the PT dual to the pentagrid. Hence each vertex of the PT corresponds to a mesh in the pentagrid and is defined by a set of five integers $\{k_j\}$.

Consider now an edge (of a rhombus in de Bruijn's tiling) which is directed along $\boldsymbol{\nu}_j$ $(0 \leqslant j \leqslant 4)$. We then note that the tiling contains infinite strips of adjacent rhombi, each having two edges parallel to $\boldsymbol{\nu}_j$. Such a strip is shown in figure 3($a$). One can define the image of the strip in the pentagrid picture (figure 3($b$)). It consists of intersections of a particular line of the $j$th set with lines of other sets; each intersection of the former with a line of the $l$th set $(l \neq j)$ may be mapped back to a rhombus whose edges are directed along $\boldsymbol{\nu}_j$ and $\boldsymbol{\nu}_l$. Thus, the strip is completely defined by its sequence of intersections with the lines of the other sets (de Bruijn 1981a, b). Below we shall study in some detail these sequences and classify the various structures that occur along this line.

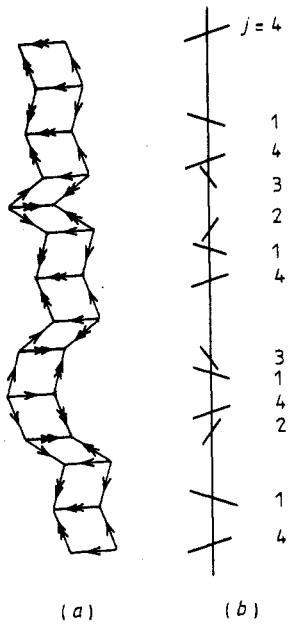


**Figure 3.** ($a$) An infinite strip of the $j = 0$ set. ($b$) Its image in the pentagrid picture.

To be more specific let us select a particular line of the $j = 0$ set and denote it as a reference line (RL) (figure 4($a$)). An intersection of the RL with a $j = 1$ line, i.e. a line that belongs to the $j = 1$ set (a $j = 4$ line) is dual to a T-tile whose edges are along $\boldsymbol{\nu}_0$ and $\boldsymbol{\nu}_1$ ($\boldsymbol{\nu}_0$ and $\boldsymbol{\nu}_4$). Similarly any intersection with a $j = 2$ line ($j = 3$ line) is dual to a t-tile whose edges are along $\boldsymbol{\nu}_0$ and $\boldsymbol{\nu}_2$ ($\boldsymbol{\nu}_0$ and $\boldsymbol{\nu}_3$). Choosing the distance between

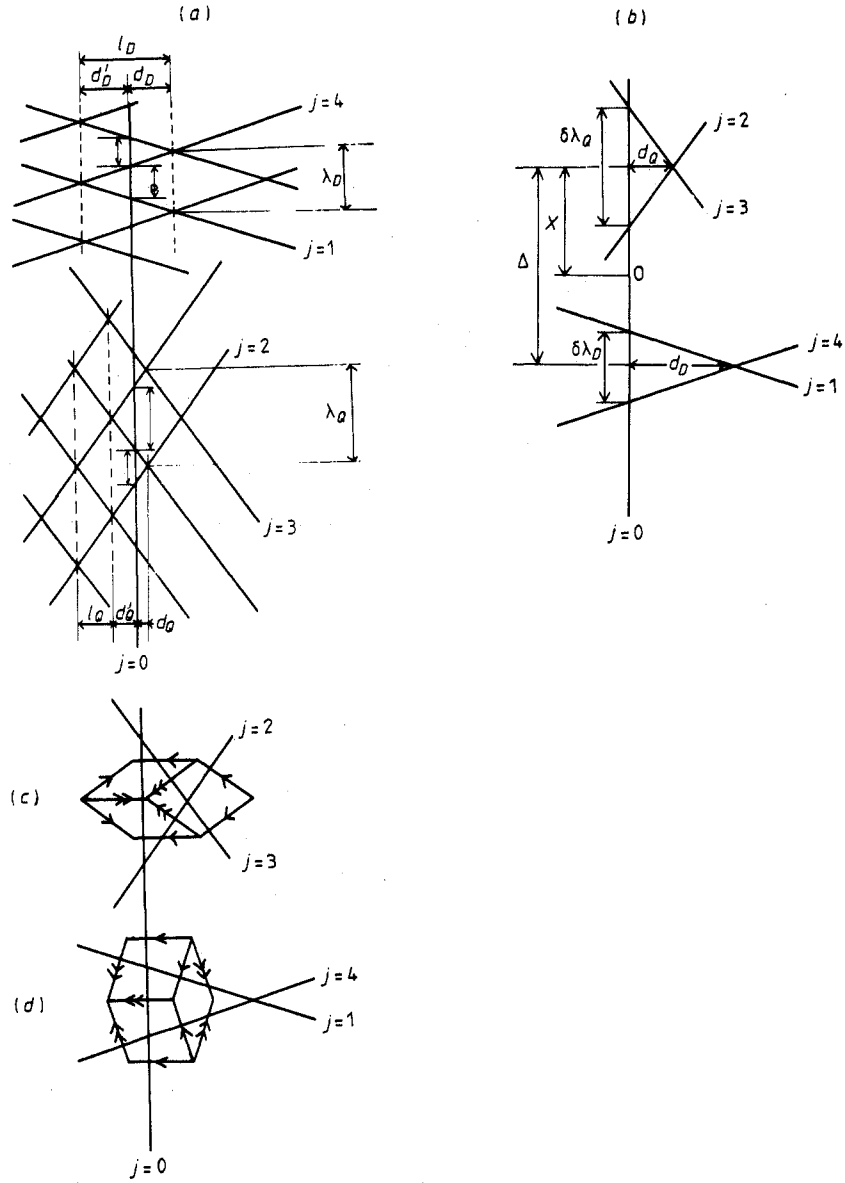


**Figure 4.** Intersections of a reference line RL with other pentagrid lines (not all the intersections are shown). (*a*) Various periods along the RL. (*b*) Geometrical parameters which characterise various meshes. (*c*) A hexagon of type $H_Q$. (*d*) A hexagon of type $H_D$.

two consecutive parallel lines to be equal to 1, the distance on the RL between two intersections with consecutive lines of the $j=1$ set is (see figure 4(*a*))

$$\lambda_D = (\sin 72)^{-1}. \tag{2.5a}$$

$\lambda_D$ corresponds also to the distance between two intersections of the RL with two consecutive lines of the $j=4$ set (see figure 4(*a*)).

Similarly, we have for the distance between two intersections of the RL with consecutive lines of the $j=2$ (or $j=3$) set (figure 4($a$))

$$\lambda_Q = (\sin 36)^{-1}. \tag{2.5b}$$

We note that

$$\lambda_D/\lambda_Q = \tau^{-1} \tag{2.5c}$$

where $\tau = (1+\sqrt{5})/2$ is the golden ratio†.

We now recall that a pentagrid is defined by five real numbers $(\gamma_j)_{j=0,\ldots,4}$, such that the relation (2.2) is obeyed. In this section we shall introduce more convenient parameters and enumerate the degrees of freedom in the construction of the pentagrid. Let us consider intersections between the lines of the $j=1$ set with the lines of the $j=4$ set. These intersections are along equidistant lines, parallel to the $j=0$ set, whose spacing is $l_D = \tau$ (see the broken lines in figure 4($a$)). Let $d_D$ be the distance between the RL and the vertical line defined by the intersections of sets $j=1$ and $j=4$ (hereafter denoted (1, 4)), which is the closest to the RL on its right side (see figure 4($a$)), and let $d'_D$ be the distance between the RL and the vertical line defined by the intersections of sets $j=1$ and $j=4$, which is the closest to the RL on its left side. It is easy to see that

$$l_D \equiv d_D + d'_D = \tau. \tag{2.6a}$$

$d_Q$ and $d'_Q$ are chosen in a similar way, for the intersections of lines of the $j=2$ set and lines of the $j=3$ set. They satisfy

$$l_Q \equiv d_Q + d'_Q = \tau^{-1} \tag{2.6b}$$

where $l_Q$ is the distance between two consecutive lines (parallel to the RL) along which sets $j=2$ and $j=3$ intersect (see figure 4($a$)).

One can see in figure 4($b$) that, if we consider the intersections (1, 4) which are the closest to the RL on its right (on its left), the corresponding lines of the $j=1$ and $j=4$ sets cut the RL along intervals $\delta\lambda_D(\delta\lambda'_D)$. Here, $\delta\lambda_D$ represents the interval which is the base of a triangular mesh, whose sides are segments of a line of the $j=1$ set and a line of the $j=4$ set, such that the apex of this triangle is to the right of the RL. $\delta\lambda'_D$ is the base of a triangle whose sides are also segments of a line of the $j=1$ set and of a line of the $j=4$ set, but in this case the apex is to the left side of the RL. It is easy to show that

$$\begin{aligned} \delta\lambda_D &= 2d_D \tan 18 \qquad & \delta\lambda_Q &= 2d_Q \tan 54 \\ \delta\lambda'_D &= 2d'_D \tan 18 \qquad & \delta\lambda'_Q &= 2d'_Q \tan 54 \end{aligned} \tag{2.7}$$

where $\delta\lambda_Q$ and $\delta\lambda'_Q$ are defined similarly to $\delta\lambda_D$ and $\delta\lambda'_D$ for (2, 3) intersections.

The pentagrid is defined by (2.1) with an arbitrary origin O. If we change the origin from point O to point O′, we have

$$(\mathbf{OO}+\mathbf{O'M})\cdot\boldsymbol{\nu}_j + \gamma_j = k_j.$$

Hence, the new pentagrid is defined by $(\gamma'_j)_{j=0,\ldots,4}$ such that

$$\gamma'_j = \gamma_j + \mathbf{OO'}\cdot\boldsymbol{\nu}_j. \tag{2.8}$$

We see that the choice of an origin corresponds to two degrees of freedom. This follows from the fact that the vector $\mathbf{OO'}$ is two dimensional. Let us therefore choose

† The subscripts $Q$ and $D$ follow de Bruijn's notation for the various types of vertices in the PT.

a particular origin O taken in between two neighbouring intervals $\delta\lambda_D$ and $\delta\lambda_Q$, on some particular RL identified by $j=0$, such that $\gamma_0=0$. Now the pentagrid is entirely defined by three quantities related to the particular RL we consider, namely $d_Q$, $d_D$ and $\Delta$, where $\Delta$ measures a distance between two neighbouring intervals $\delta\lambda_D$ and $\delta\lambda_Q$ on the RL. We have the following correspondence between $\gamma_i$ $(i=0,1,2,3,4)$ and $\delta\lambda_D$, $\delta\lambda_Q$, $X$, $\Delta$:

$$\begin{aligned}
\gamma_0 &= 0 \\
\gamma_1 &= \left(\Delta - X - \frac{\delta\lambda_D}{2}\right)\cos 18 \\
\gamma_2 &= -\left(X - \frac{\delta\lambda_Q}{2}\right)\cos 54 \\
\gamma_3 &= \left(X + \frac{\delta\lambda_Q}{2}\right)\cos 54 \\
\gamma_4 &= -\left(\Delta - X + \frac{\delta\lambda_D}{2}\right)\cos 18
\end{aligned} \tag{2.9}$$

where $X$ is the distance between the origin O and the middle point of the interval $\delta\lambda_Q$ (figure 4($b$)).

When we set $C$ in (2.2) to be equal to 0, we obtain from (2.9) that

$$\frac{\delta\lambda_D}{\delta\lambda_Q} = \frac{\cos 54}{\cos 18} = \frac{1}{\tau}. \tag{2.10}$$

By (2.5) and (2.7) we have

$$\frac{\delta\lambda_D}{\lambda_D} = \frac{2d_D \tan 18}{(\sin 72)^{-2}} = 2d_D \cos 72 = \frac{d_D}{\tau} \tag{2.11$a$}$$

and

$$\frac{\delta\lambda_Q}{\lambda_Q} = \frac{2d_Q \tan 54}{(\sin 35)^{-2}} = 2d_Q \cos 36 = \tau d_Q. \tag{2.11$b$}$$

Combining the previous three equations we obtain

$$\frac{\delta\lambda_D}{\lambda_D} = \frac{\delta\lambda_Q}{\lambda_Q} = \frac{d_D}{\tau} = \tau d_Q. \tag{2.12}$$

This shows that $d_Q$ is determined by the choice of $d_D$. *Only two quantities are independent*: $d_D$ and $\Delta$.

Consider now how the distance $d_D$ varies as we proceed from one line of the $j=0$ set to the next. As already stated, $l_D=\tau$ (2.6$a$). Since two consecutive lines of the $j=0$ set are a unit distance apart, $d_D$ for the next $j=0$ lines is defined in the following way: let us denote by $d_D^n$ the heights of the triangles bound by lines of the $j=1$ and the $j=4$ sets, whose base is on the $n$th line of the set $j=0$. Then

$$d_D^n = m\tau - n \tag{2.13}$$

where $m$ is chosen such that $0<d_D^n<\tau$. That is $d_D^n = m\tau \pmod 1$. According to the theory of irrational numbers (Niven 1956), it follows that $d_D$ is densely and uniformly distributed between 0 and $l_D=\tau$. Similarly $d_Q$ is densely and uniformly distributed between 0 and $l_Q=\tau^{-1}$.

At this point we would like to describe the configurations along the RL for different values of $d_D$ between 0 and $\tau$. We start by stating some results concerning configurations on the RL in the pentagrid, and then turn to the dual geometry in the PT.

An important component in the configurations that arise along the strip dual to the RL are triangular meshes whose bases are on the RL and whose sides are segments of lines of the sets $j=1$ and $j=4$. As shown in figure 4($c$), the dual of such a triangle is an hexagon containing two tiles of type T and a tile of type t. We denote these hexagons by $H_D$ since the central vertex is a $D$ (deuce) in de Bruijn's notation (de Bruijn 1981a, b). Similarly a triangular mesh bounded by the RL and segments of lines $j=2$ and $j=3$ is dual to an hexagon $H_Q$ containing two tiles of type t and a tile of type T (see figure 4($d$)).

We will now show that when $0<d_D<1$, a segment $\delta\lambda_Q$ ($\delta\lambda_D$) which does not overlap with a segment $\delta\lambda_D$ ($\delta\lambda_Q$) is the base of a triangular mesh. In other words, a triangle whose base is $\delta\lambda_D$ ($\delta\lambda_Q$) is not intersected by any line of the pentagrid. This means that the configuration dual to a $\delta\lambda_D$ ($\delta\lambda_Q$) interval will be a hexagon of type $H_D$ ($H_Q$).

This assertion is easily proved for the intervals $\delta\lambda_Q$. In figure 5($a$), we have drawn such an interval. We can easily see that the relative slopes of the lines imply that if a line of the $j=1$ or the $j=4$ sets cuts the triangle ABC, it necessarily cuts the segment AB, and the intervals $\delta\lambda_D$ and $\delta\lambda_Q$ are overlapping.

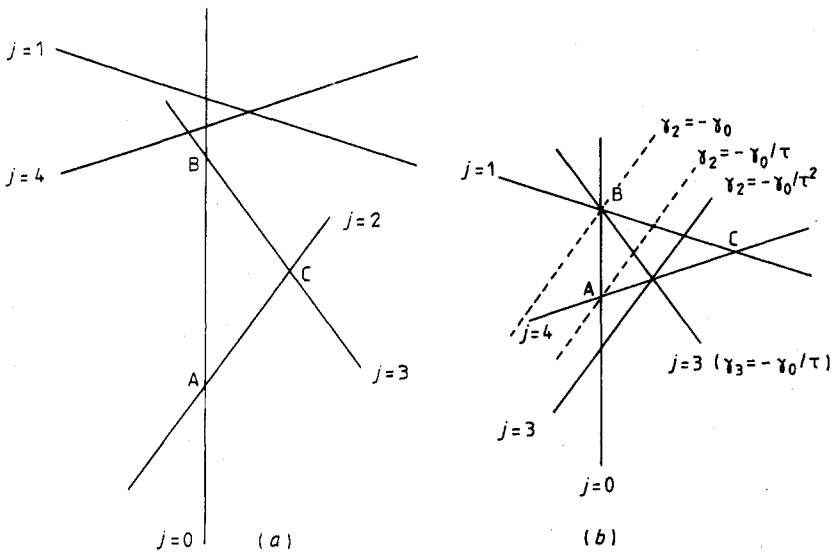


**Figure 5.** ($a$) A triangular mesh based on $\delta\lambda_Q$. ($b$) A triangular mesh bounded by $\delta\lambda_D$ and other lines.

The case of the $\delta\lambda_D$ overlapping intervals is slightly more subtle. Figure 5($b$) shows a triangle ABC, based on $\delta\lambda_D \equiv$ AB. Let us choose the origin at C. Then $\gamma_1=\gamma_4=0$. Let us suppose that a line of the set $j=3$ cuts the triangle ABC along the edge BC, without crossing the edge AB. We easily see that if the $j=3$ line passes through the point B, then $\gamma_3=-\gamma_0/\tau$ (here $\gamma_0<0$), and if the $j=3$ line passes in C, then $\gamma_3=0$. Since $\Sigma_{j=0}^{4}\gamma_i=0$, we have $\gamma_2=(-\gamma_0-\gamma_3)$, and we can draw the corresponding line of the $j=2$ set. In fact when $0<\gamma_3<-\gamma_0/\tau$, we have $-\gamma_0/\tau^2<\gamma_2<-\gamma_0$. In the interval

$-\gamma/\tau < \gamma_2 < -\gamma_0$, the line of the $j=2$ set cuts the segment AB. When $-\gamma_0/\tau^2 < \gamma_2 < -\gamma_0/\tau$, the interval $\delta\lambda_D$ is inside the interval $\delta\lambda_Q$. Hence we have shown that when the interval $\delta\lambda_D$ is not overlapping and not contained inside $\delta\lambda_Q$, it is the base of a triangular mesh.

In the case $\tau^{-1} < d_D < \tau$, we have to consider $0 < d'_D = \tau - d_D < 1$, and we get similar results, i.e. an interval $\delta\lambda'_D$ ($\delta\lambda'_Q$) which does not intersect a $\delta\lambda'_Q$ ($\delta\lambda'_D$) interval is the base of a triangular mesh.

Figure 6 shows the structures that may occur along the RL as $d_D$ increases from 0 to $\tau$.

(*a*) $0 < d_D < \tau^{-1}$. Triangular meshes of bases $\delta\lambda_Q$ or $\delta\lambda_D$ appear only on the right side of the RL. In fact in this case $1 < d'_D < \tau$; this implies immediately that triangular meshes of base $\delta\lambda'_D$ cannot exist since $d'_D$ is larger than 1. In order to prove now that a triangle of base $\delta\lambda'_Q$ cannot show up, we note that the total minimal length of two non-overlapping intervals $\delta\lambda'_Q$ and $\delta\lambda'_D$, namely $\delta\lambda'_Q + \delta\lambda'_D$ (see figure 7) cannot be larger than the periodicity at which $\delta\lambda'_D$ intervals appear, which is $\lambda_D$. But since

$$\frac{\delta\lambda'_Q + \delta\lambda'_D}{\lambda_D} = \tau d'_D > 1 \tag{2.14}$$

we see that such a configuration, where $\delta\lambda_D$ and $\delta\lambda_Q$ do not overlap, is not possible.

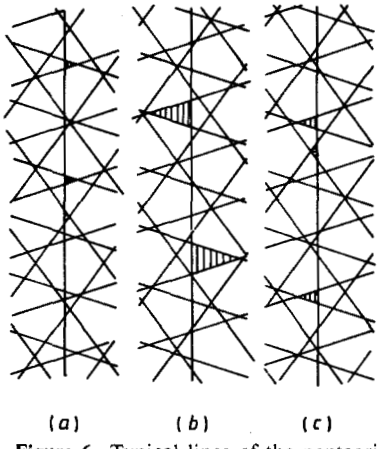


**Figure 6.** Typical lines of the pentagrid, with $d_D$ varying from 0 to $\tau$. (*a*) $0 < d_D < \tau^{-1}$. (*b*) $\tau^{-1} < d_D < 1$. (*c*) $1 < d_D < \tau$. (In each case some of the triangular meshes are darkened).

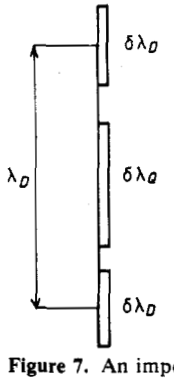


**Figure 7.** An impossible configuration (cf (2.14)).

(*b*) $\tau^{-1} < d_D < 1$. Triangular meshes of base $\delta\lambda_D$ and $\delta\lambda'_D$ appear. Equation (2.14) still holds; we also notice that, similarly

$$\frac{\delta\lambda_D + \delta\lambda_Q}{\lambda_D} = \tau d_D > 1. \tag{2.15}$$

Therefore triangles of bases $\delta\lambda_Q$ and $\delta\lambda'_Q$ do not show up in this range of values of $d_D$.

(*c*) $1 < d_D < \tau$. Triangular meshes appear only on the left side of the RL. The heights of those triangles are $d'_D$ and $d'_Q$.

We analyse now the dual structures of figure 6 in the PT. Let us first suppose, as in case (*a*) above that $0 < d_D < \tau^{-1}$. Then we have the following.

(*a*1) A triangle of base $\delta\lambda_Q$, whose edges are segments of lines of the $j = 2$ set and of the $j = 3$ set, is dual to a hexagon $H_Q^R$, depicted in figure 8(*a*). The index R in $H_Q^R$ indicates a hexagon of type $Q$ (see above) whose dual triangle appears on the right-hand side of the RL.

(*a*2) A triangle of base $\delta\lambda_D$, whose edges are segments of lines of the $j = 1$ and of the $j = 4$ sets, is dual to a hexagon $H_D^R$ (figure 8(*b*)).

(*a*3) The interval $\delta\lambda_D$ is contained in the interval $\delta\lambda_Q$; the dual structure is a decagon $D_s^R$ (figure 8(*c*)) (with a reflection symmetry about a line perpendicular to the RL).

(*a*4) When the intervals $\delta\lambda_D$ and $\delta\lambda_Q$ are overlapping, the dual configuration is a decagon $D_a^R$ lacking the above symmetry: $\delta\lambda_D$ is not contained in $\delta\lambda_Q$ (cf figures 8(*d*) and 8(*e*)).

Similar considerations apply when $1 < d_D < \tau$ (case (*c*) above), but one has to consider intervals $\delta\lambda'_D$ and $\delta\lambda'_Q$. The dual hexagons and decagons are then left sided: $H_D^L$, $H_Q^L$, $D_a^L$, $D_s^L$.

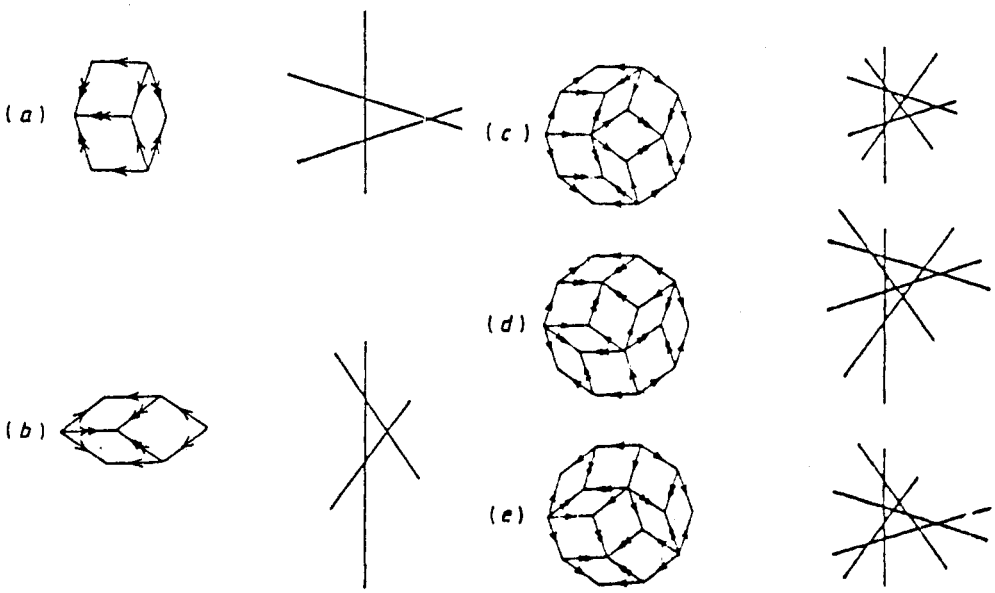


**Figure 8.** Different configuration of the intervals $\delta\lambda_Q$ and $\delta\lambda_D$ and their dual figures in the tiling. The central vertices of the hexagons are $Q$ and $D$ vertices in de Bruijn's nomenclature. (*a*) A hexagon $H_D^R$ dual of $\delta\lambda_Q$. (*b*) A hexagon $H_D^R$ dual of $\delta\lambda_D$. (*c*) A decagon dual to $\delta\lambda_D$ and $\delta\lambda_Q$ overlapping. (*d*), (*e*) Decagons dual to $\delta\lambda_D$ nested within $\delta\lambda_Q$.

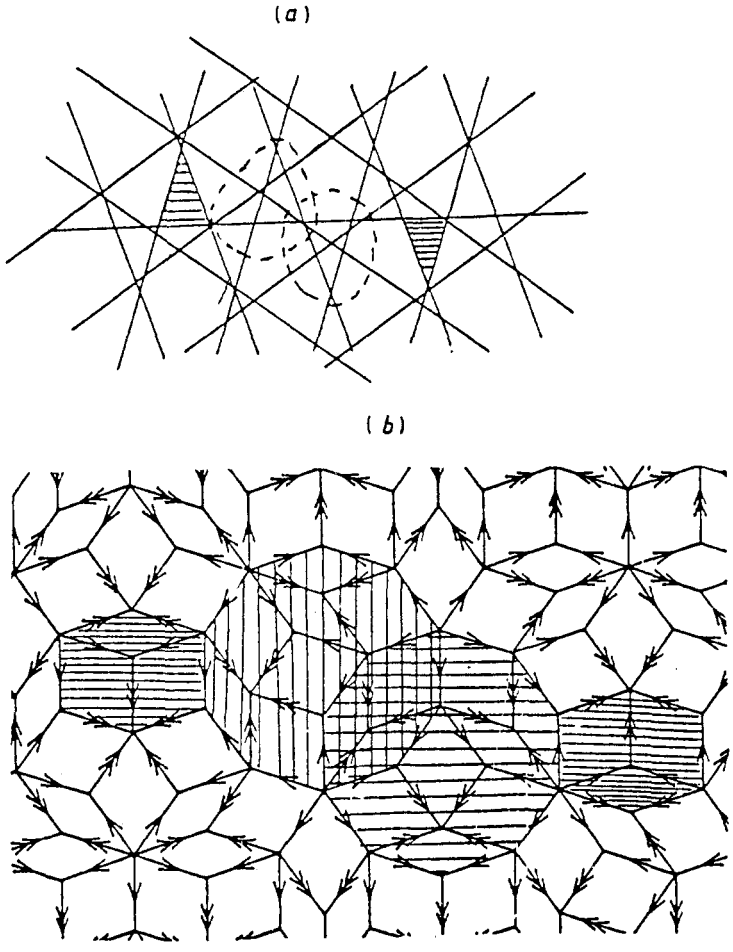


**Figure 9.** (*a*) A strip satisfying $\tau^{-2} < d_D < 1$, in the pentagrid, (*b*) the image of (*a*) in the tiling. We see that left-sided configurations are separated from right-sided configuration by interpenetrating decagons.

The case $\tau^{-1} < d_D < 1$ (discussed in (*b*) above), is more delicate. Equations (2.14) and (2.15) show that only non-overlapping $\delta\lambda_D$ and $\delta\lambda'_D$ intervals may appear. They give rise respectively to $H_D^R$ and $H_D^L$. Figure 9(*a*, *b*) shows such a line in the pentagrid and in the tiling. A careful examination shows that right-sided configurations are separated from left-sided configurations by two *interpenetrating decagons.*

In summary, in § 2 we have established a description of the pentagrid in terms of parameters $\delta\lambda_D$, $\delta\lambda_Q$, $d_D$ and $d_Q$. In order to analyse the different configurations that occur along the RL, we have to consider the intervals $\delta\lambda_D$ ($\delta\lambda_Q$): if $\delta\lambda_D$ ($\delta\lambda_Q$) does not overlap with $\delta\lambda_Q$ ($\delta\lambda_D$), the dual configuration is a hexagon; if $\delta\lambda_D$ does overlap with $\delta\lambda_Q$, the dual configuration is a decagon.

## 3. Length and contents of a worm

In this section we will calculate the densities of different structures (hexagons, decagons) which appear along a RL. A special attention will be given to 'worm' configurations.

A worm consists of a succession of adjacent hexagons bounded by two decagons (cf figure 10).

### *3.1. Worms along pentagrid lines, such that $0 < d_D < \tau^{-1}$*

A hexagon $H_D^R$ ($H_Q^R$) appears when an interval $\delta\lambda_D$ ($\delta\lambda_Q$) does not overlap with another interval $\delta\lambda_Q$ ($\delta\lambda_D$) along the RL. Suppose we start from a configuration where the two intervals $\delta\lambda_D$ and $\delta\lambda_Q$ overlap. This corresponds to the endpoint of a worm, which is a decagon. Suppose moreover that the distance between the projection on the RL of the points of intersection of (1, 4) and (2, 3) is $\Delta$ (figure 4($b$)). Starting from this configuration, we propagate the projections of the (1, 4) and (2, 3) intersections (with periodicities $\lambda_D$ and $\lambda_Q$ correspondingly) along the RL. The corresponding triangles overlap for the first time after $n$ periods of $\lambda_D$ and $m$ periods of $\lambda_Q$, i.e. their dual is an end decagon which bounds a worm of length $(m+n-2)$ (i.e. $(m-1)H_Q$ and $(n-1)H_D$ along the worm). This happens when the following inequality is satisfied:

$$|\Delta + m\lambda_Q - n\lambda_D| < \frac{\delta\lambda_D + \delta\lambda_Q}{2} = \frac{\tau d_D \lambda_D}{2} \tag{3.1a}$$

($m$ and $n$ are integers) with the minimal value of $(n+m)$. Dividing this equation by $\lambda_D$ we obtain

$$|x + m\tau - n| < \frac{\tau d_D}{2}. \tag{3.1b}$$

An analysis of (3.1$b$) is presented in the appendix. The proof of (3.1) relies on some standard theorems of measure theory. It then follows that for the range of values of

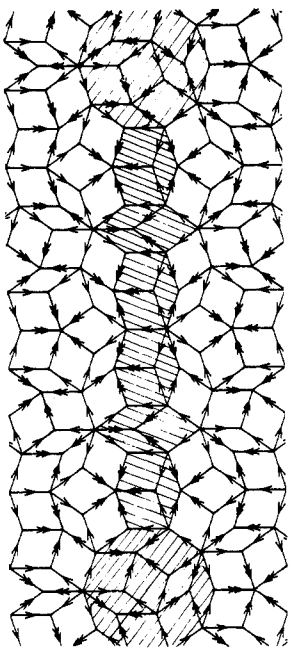

**Figure 10.** A worm along a pentagrid line with $0 < d_D < \tau^{-2}$.

$d_D$ defined by

$$\tau^{-(p+1)} < d_D < \tau^{-p} \tag{3.2}$$

$p$ being a positive integer, the allowed values of $(n, m)$ are

$$(f_{p+1}, f_p) \qquad (f_{p+2}, f_{p+1}) \qquad (f_{p+3}, f_{p+2}) \tag{3.3a}$$

which means that only three lengths of worms are allowed for a given line: each worm consists of $(f_{i+2}-2)$ hexagons: $(f_{i+1}-1)$ of type $H_D$ and $(f_i-1)$ of type $H_Q$ ($i = p, p+1$ or $p+2$).

The case when $d_D$ is equal to a value $\tau^{-p}$ is also discussed in the appendix: in such a case, there are only two allowed values of $(n, m)$, which are

$$(f_{p+1}, f_p) \qquad (f_{p+2}, f_{p+1}). \tag{3.3b}$$

If we introduce

$$\omega = \frac{\delta\lambda D + \delta\lambda_Q}{\lambda_D} = \tau d_D \qquad \text{and} \qquad \mu = \tau^{-p+1} - \omega \tag{3.4}$$

we can obtain the relative weights of worms of different lengths. They are summarised in table 1. We note that $\mu$ is between 0 and $\tau^{-p-1}$.

By relative weight we mean the number of worms of a given length, divided by the total number of worms, in an arbitrary large length of the RL (see the appendix). The worms corresponding to $\mu = 0$ cases do not contribute to the relative weights: they form a set of zero measure.

### *3.2. Concentration of hexagons and decagons along a strip*

As we have seen, a strip might be described either as a succession of one-sided decagons and hexagons (this is the case when $0 < d_D < \tau^{-1}$ or $1 < d_D < \tau$), or as a succession of two-sided hexagons and decagons separated by interpenetrating decagons when $\tau^{-1} < d_D < 1$. We shall employ in this section the pentagrid representation in order to calculate the densities of these geometrical creatures. Let us consider the intervals $\delta\lambda_D$ and $\delta\lambda_Q$ plotted in figure 11($a$) within a segment of length $\lambda_D$. The expectation value of the

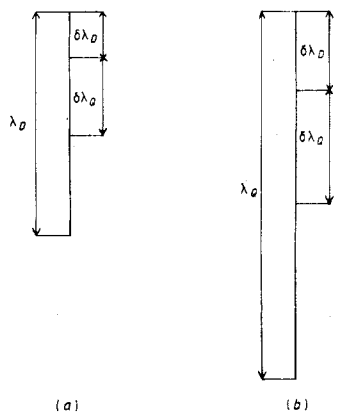


**Figure 11.** Sequence of intersections along the RL. ($a$) $\delta\lambda_D$ and $\delta\lambda_Q$ intervals along the RL compared with $\lambda_Q$. ($b$) $\delta\lambda_D$ and $\delta\lambda_Q$ intervals along the RL compared with $\lambda_D$.

number of centres of $\delta\lambda_Q$ intervals in an interval of length $\lambda_D$ is $\lambda_D/\lambda_Q$. By definition, in each period $\lambda_D$, there is one interval $\delta\lambda_D$ corresponding to a right hexagon of type $D$: $H_D^R$. Therefore the remaining space available for centres of $\delta\lambda_Q$ intervals, which do not overlap with $\delta\lambda_D$ (i.e. correspond to $H_Q^R$) is $\lambda_D - \delta\lambda_D + \delta\lambda_Q$. Therefore the density of $H_Q^R$, $\rho_R(Q)$, per unit length along a grid line is

$$\rho_R(Q) = \frac{1}{\lambda_D}\,\frac{\lambda_D}{\lambda_Q}\,\frac{\lambda_D - (\delta\lambda_D + \delta\lambda_Q)}{\lambda_D} = \frac{1 - d_D\tau}{\lambda_Q}. \tag{3.5a}$$

Consider now the intervals $\delta\lambda_D$ and $\delta\lambda_Q$ of figure 10($b$) plotted along an interval of length $\lambda_Q$ for the case $0 < d_D < 1$. By the same argument, we calculate the density $\rho_R(D)$ of $H_D^R$

$$\rho_R(D) = \frac{1}{\lambda_Q}\,\frac{\lambda_Q}{\lambda_D}\,\frac{\lambda_Q - (\delta\lambda_D + \delta\lambda_Q)}{\lambda_Q} = \frac{1 - d_D}{\lambda_D} \tag{3.5b}$$

and the density $\rho_R(D, Q)$ of overlapping intervals of width $\delta\lambda_D$ and $\delta\lambda_Q$, i.e. of decagons, is

$$\rho_R(D, Q) = \frac{\delta\lambda_D + \delta\lambda_Q}{\lambda_D\lambda_Q} = \frac{d_D}{\lambda_D}. \tag{3.5c}$$

Left hexagons are obtained by changing $d_D$ into $\tau - d_D = d'_D$ which yields

$$\rho_L(Q) = \frac{\tau(d_D - 1)}{\lambda_Q} \tag{3.6a}$$

$$\rho_L(D) = \frac{d_D - (\tau - 1)}{\lambda_D} \tag{3.6b}$$

$$\rho_L(D, Q) = \frac{\tau - d_D}{\lambda_D}. \tag{3.6c}$$

As expected, $H_D^L$ and $H_Q^L$ coexist in worms that correspond to $1 < d_D < \tau$, while only $H_D^R$ and $H_D^L$ appear for $\tau^{-2} < d_D < 1$.

### *3.3. Statistics of worms*

Let us denote by $C(L_i)$ the number of worms containing $(L_i)$ hexagons, divided by the total number of worms along the RL. We have $L_i = f_i - 2$; the worms contain $(f_{i-1} - 1)H_D$ hexagons and $(f_{i-2} - 1)H_Q$ hexagons. (We have $f_0 = 0, f_1 = 1, f_2 = 1, f_3 = 2$, etc). $i = 3$ gives $C(0)$; this is the density of worms of zero length, i.e. pairs of consecutive decagons. $i = 4$ gives $C(1)$; these worms contain on $H_D$ hexagon and no $H_Q$ hexagons. $i = 5$ corresponds to $C(3)$ which are worms containing one $H_Q$ hexagon and two $H_D$ hexagons.

Table 1 gives the relative weight of worms of a given length, for a fixed $\omega$ and $\mu$. Let us calculate the contribution to $C(f_i - 2)$ of an interval

$$\tau^{-p} < \omega < \tau^{-p+1}. \tag{3.7}$$

**Table 1**

| Worm size | Number of hexagons $D$ | Number of hexagons $Q$ | Relative weight |
|---|---|---|---|
| $f_{p+2}-2$ | $f_{p+1}-1$ | $f_p-1$ | $\dfrac{\tau^{-p-1}-\mu}{\omega}$ |
| $f_{p+3}-2$ | $f_{p+2}-1$ | $f_{p+1}-1$ | $\dfrac{\tau^{-p}-\mu}{\omega}$ |
| $f_{p+4}-2$ | $f_{p+3}-3$ | $f_{p+2}-1$ | $\dfrac{\mu}{\omega}$ |

This contribution is zero unless $i=p+2$, $p+3$ or $p+4$. In other words, the interval (3.7) above gives contributions to three lengths of worms. We have

$$C'(f_{p+2}-2)=\int_0^{\tau^{-p-1}}\frac{\tau^{-p-1}-\mu}{\tau^{-p+1}-\mu}\,d\mu=\tau^{-p-1}(1-\tau\ln\tau) \tag{3.8a}$$

$$C''(f_{p+3}-2)=\int_0^{\tau^{-p-1}}\frac{\tau^{-p}-\mu}{\tau^{-p+1}-\mu}\,d\mu=\tau^{-p-1}(1-\ln\tau) \tag{3.8b}$$

$$C'''(f_{p+4}-2)=\int_0^{\tau^{-p-1}}\frac{\mu}{\tau^{-p+1}-\mu}\,d\mu=\tau^{-p-1}(\tau^2\ln\tau-1). \tag{3.8c}$$

One checks that $C'(f_{p+2}-2)+C''(f_{p+3}-2)+C'''(f_{p+4}-2)=\tau^{-p-1}$, which is the range of variation of $\mu$. Now the density $C(f_i-2)$ of the worms of length $f_i-2$ is obtained as the sum of three such contributions, with $p=i-2$, $i-3$, $i-4$, i.e.

$$C(f_i-2)=C'(f_i-2)+C''(f_i-2)+C'''(f_i-2). \tag{3.9}$$

This gives

$$C(f_i-2)=\sqrt{5}\,\tau^{-i+2}\ln\tau \qquad i\geqslant 5 \tag{3.10a}$$

with special expressions for $C(0)$ and $C(1)$

$$C(0)=\frac{1}{\tau^2}(1-\tau\ln\tau) \qquad i=3 \tag{3.10b}$$

$$C(1)=\frac{1}{\tau^2}(\tau-2\ln\tau) \qquad i=4. \tag{3.10c}$$

The contribution to $C(0)$ comes only from the interval $\tau^{-2}<\omega<1$, and we have $C(0)=C'(f_i-2)$ with $i=3$. The contributions to $C(1)$ come from the intervals $\tau^{-2}<\omega<1$ and $\tau^{-2}<\omega<\tau^{-2}$; we have $C(1)=C''(f_i-2)+C'(f_i-2)$, with $i=4$.

We can check that $\Sigma_{i\geqslant 3}\,C(f_i-2)=1$ (note that $\Sigma_{i\geqslant 5}\,C(f_i-2)=(\tau+2)\tau^{-2}\ln\tau$).

Solving (3.1) we have shown that worms are made of $L_p$ hexagons with $L_p=f_p-2$. Asymptotically $L_p$ goes like $\tau^p$. Equation (3.10$a$) shows that $C(L_p)$ goes like $\tau^{-p}$.

Let us choose a hexagon at random in the tiling. The probability that this hexagon belongs to a worm of length $L_p$ is $P(L_p)=L_pC(L_p)$. Asymptotically this quantity does not depend on $p$. Hence a hexagon, chosen at random, has (roughly) equal probabilities to belong to a worm of any length (provided the worm is long enough).

Let us consider a finite tiling of size $R \sim \tau^n$ and let us choose at random a hexagon in it. This hexagon belongs to a worm of size $L_p$. The weighted average of the length of these worms can be calculated using the probability defined above. We have

$$\langle L \rangle = \frac{\Sigma_p L_p P(L_p)}{\Sigma_p P(L_p)} = \frac{\Sigma_p L_p^2 C(L_p)}{\Sigma_p L_p C(L_p)} \sim \frac{\tau^n}{n} \tag{3.11}$$

where we have used the expressions of $L_p$ and of $C(L_p)$. If we introduce $R \sim \tau^n$, we find that

$$\langle L \rangle = \frac{R}{\ln R}. \tag{3.12}$$

$\langle L \rangle$ is the average size of the worm to which a hexagon chosen at random belongs.

### *3.4. Decagons*

As indicated above, when intervals $\delta\lambda_D$ and $\delta\lambda_Q$ overlap along a line of the grid, the dual figure in the PT is a decagon.

$D_R$ (right decagons) are shown (figures 8(*c*, *d*, *e*)) both in the pentagrid and in the PT. The frequency of $D$ can be calculated by a method akin to that of § 3.3. Consider $0 < d_D < 1$ (figure 11(*a*)). The average number of centres of $\delta\lambda_D$ in the period $\lambda_Q$ is $\lambda_Q/\lambda_D$. We will obtain a decagon of the type shown in figure 8(*c*) when $\delta\lambda_D$ is included in $\delta\lambda_Q$. The frequency of this configuration is $(\delta\lambda_Q - \delta\lambda_D)/\lambda_Q$. Hence, the density of these decagons ($D_s$) is

$$\rho_R(D_s) = \frac{1}{\lambda_Q}\frac{\lambda_Q}{\lambda_D}\frac{\delta\lambda_Q - \delta\lambda_D}{\lambda_Q} = \frac{\tau^{-3} d_D}{\lambda_D}. \tag{3.13}$$

The total density of $D$ is given by equation (3.5*c*). By subtraction we obtain, for the decagons shown in figures 8(*d*) and 8(*e*),

$$\rho_R(D_a) = 2\tau^{-2}\frac{d_D}{\lambda_D}. \tag{3.14}$$

Densities for $D_a^L$ and $D_s^L$ on lines for which $1 < d_D < \tau$ are obtained by substituting $d'_D = \tau - d_D$.

The situation for lines for which $\tau^{-2} < d_D < 1$ is slightly different, and is shown in figure 9(*a*, *b*). Two consecutive hexagons are separated by a pair of decagons with a common part (a double decagon); one of these decagons is a $H_D^R$ and is on the right side of the RL; the other one is a $H_D^L$ and is on the left side of the RL. Their densities have been calculated above.

## 4. General remarks on excitations of the PT in connection with worms

Different ways of analysing the PT, i.e. the cut-and-projection method (de Bruijn 1981, Duneau and Katz 1985, Katz and Duneau 1986), the Landau-Guinzburg formalism (Biham *et al* 1986) and the group theoretical approach (Bak 1985, Alexander 1986) show that its elementary excitations are phonons and phasons. Moreover using the cut-and-projection formalism, the existence of a third non-hydrodynamical mode has been established (Kléman *et al* 1986). This mode consists of local rearrangements around the vertices. As already stated in § 1, it introduces new tiles t′ and T′ (figure 1(*d*)), and corresponds to a structural transformation.

Since these modes are better understood by the cut-and-projection formalism than in the pentagrid picture, and since in any case some knowledge of the five-dimensional representation of the PT is required for the following, we give now some ingredients of this formalism. A more detailed account can be found in de Bruijn (1981a, b) and Pavlovitch and Kléman (1987).

PT can be obtained from the projection of a set of vertices which belong to a simple cubic hyperlattice of unit edge in a five-dimensional space $E_5$ onto a plane $P_\parallel(\boldsymbol{\gamma})$ (the physical plane, also called parallel space) spanned by the two unit vectors $\boldsymbol{u}_1$ and $\boldsymbol{u}_2$, where

$$\begin{aligned} \boldsymbol{u}_1 &= (2/5)^{1/2} \sum_{j=0,\dots,4} \cos\frac{2\pi j}{5}\, \boldsymbol{e}_j \\ \boldsymbol{u}_2 &= (2/5)^{1/2} \sum_{j=0,\dots,4} \sin\frac{2\pi j}{5}\, \boldsymbol{e}_j. \end{aligned} \tag{4.1}$$

The vectors $\boldsymbol{e}_j = (\delta_{0j}, \delta_{1j}, \delta_{2j}, \delta_{3j}, \delta_{4j})$ form the canonical basis of $E_5$. $P_\parallel(\boldsymbol{\gamma})$ passes through the point of coordinates $(\gamma_i)_{i=0,\dots,4}$. The vertices which are projected are restricted to a strip bounded by $P_\parallel$ and another 2-plane parallel to $P_\parallel$ and at a distance $\sqrt{5}$ of it along the main diagonal $D$, directed along

$$\boldsymbol{u}_0 = (1/5)^{1/2} \sum_{j=0,\dots,4} \boldsymbol{e}_j. \tag{4.2}$$

This strip projects on the space perpendicular to $P_\parallel$ (the so-called perpendicular space) along a rhombic icosahedron. The perpendicular space itself is the external product of the (11111) diagonal of the cube, and of the plane $P_\perp$ spanned by the two unit vectors $\boldsymbol{u}_3$ and $\boldsymbol{u}_4$

$$\begin{aligned} \boldsymbol{u}_3 &= (2/5)^{1/2} \sum_{j=0,\dots,4} \cos\frac{4\pi j}{5}\, \boldsymbol{e}_j \\ \boldsymbol{u}_4 &= (2/5)^{1/2} \sum_{j=0,\dots,4} \sin\frac{4\pi j}{5}\, \boldsymbol{e}_j. \end{aligned} \tag{4.3}$$

The intersection of $P_\parallel(\boldsymbol{\gamma})$ with the hypercubic lattice planes is the pentagrid itself. The condition $\Sigma\, \gamma_j = 0$ corresponds to a special position of $P_\parallel(\boldsymbol{\gamma})$ (and of the corresponding strip), which generates a perfect PT. A generic position of $P_\parallel(\boldsymbol{\gamma})$ corresponds to a generalised PT.

We shall show that the uniform (infinite wavelength) phason mode and the uniform (infinite wavelength) structural transformation mode are located along particular worms of the tiling. These two types of modes can be described in term of (different) variations of the five quantities $(\gamma_i)_{i=0,\dots,4}$. In the pentagrid picture, they correspond to global displacements of some sets of lines.

Let us consider a tiling associated with the set $(\gamma_i)_{i=0,\dots,4}$, and introduce an excitation of the tiling $(\delta\gamma_i)_{i=0,\dots,4}$. When $(\delta\gamma_i)_{i=0,\dots,4}$ is small, not all the regions of the tiling will be affected, but only those where the displacements of the lines change the topology of the meshes in the pentagrid (figure 12). The vertices of the tiling dual to those meshes will disappear, but some other vertices will appear as we show in figures 13 and 14. The shifts of figure 13 correspond to a phason excitation, while the shifts of figure 14 correspond to a structural transformation. We see that each shift introduces two mismatches (cf Entin-Wohlman *et al* 1988).

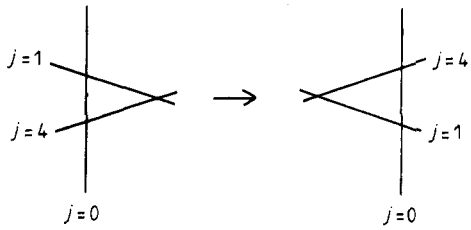


**Figure 12.** An excitation of the pentagrid which modifies the tiling. (This excitation corresponds to figure 13(*a*)).

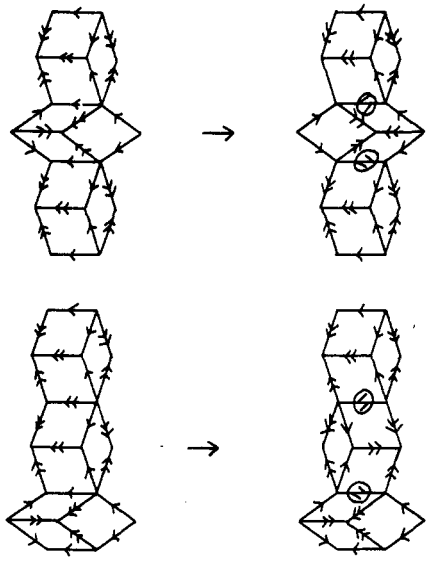

**Figure 13.** Phason excitations of hexagons. (*a*) Flipping of an hexagon $H_Q^R$ into $H_Q^L$. Two mismatches appear between the flipped hexagon and the two adjacent hexagons. (*b*) Flipping of $H_D^R$ into $H_D^L$.

From § 2, we know that with each line of the $j$th set of the pentagrid we may associate four non-independent lengths $d_D(j)$ and $d'_D(j)$, $d_Q(j)$ and $d'_Q(j)$. A change of $(\delta\gamma_i)_{i=0,\ldots,4}$ will modify $d_D(j)$, $d'_D(j)$, $d_Q$ and $d'_Q(j)$ by $\delta d_D(j)$, $\delta d'_D(j)$, $\delta d_Q(j)$ and $\delta d'_Q(j)$.

Let us consider two specific cases.

(i) An excitation $(\delta\gamma_i)_{i=0,\ldots,4}$ which preserves $\Sigma\,\delta\gamma_i = 0$. This excitation is either a phonon mode or a phason mode. Since the phonon mode corresponds to the translation of the whole pentagrid, without any change, we will consider only the phason part. This mode corresponds to $\delta\boldsymbol{\gamma} \in P_\perp$. We will consider two examples: $\delta\boldsymbol{\gamma}'_\perp = \delta\gamma'\boldsymbol{u}_3$ and $\delta\boldsymbol{\gamma}''_\perp = \delta\gamma''\boldsymbol{u}_4$, where $\delta\gamma' > 0$ and $\delta\gamma'' > 0$. We will calculate the resulting values of $\delta d_D$, $\delta d'_D$, $\delta d_Q$ and $\delta d'_Q$ for each set.

(ii) An excitation which does not preserve $\Sigma\,\delta\gamma_i = 0$ is a mixing of a phonon, a phason and a structural transformation mode. This excitation will introduce new tiles t' and T'. We will consider $\delta\boldsymbol{\gamma}''_D = \delta\gamma'''\boldsymbol{u}_0$, where $\delta\gamma''' > 0$. This choice of $\delta\boldsymbol{\gamma}$ yields a structural transformation only. As before we will calculate $\delta d_D$, $\delta d'_D$, $\delta d_Q$ and $\delta d'_Q$.

Let us consider a mesh of the pentagrid and a point $M$ belonging to this mesh. We choose a mesh which is a triangle, whose edges are segments of $j = 0$, $j = 1$ and

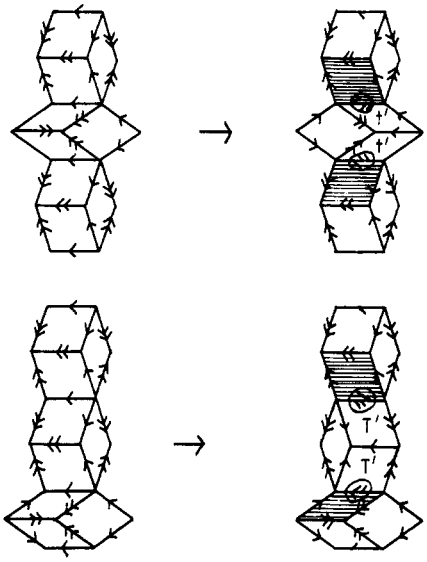


**Figure 14.** Structural transformation excitations of hexagons. (*a*) Flipping of $H_Q^R$ into an hexagon made of a tile T and two tiles t'. (*b*) Flipping of $H_D^R$ into an hexagon made of a tile t and two tiles T'. The arrowing changes accordingly along the worm.

$j=4$ set's lines such that the intersection (1, 4) is on the right of the $j=0$ set's line (see figure 15). We can introduce the vector $\boldsymbol{MH}_0$, where $H_0$ is the projection of $M$ on the line of $j=0$ set. Similarly we introduce $\boldsymbol{MH}_1$ and $\boldsymbol{MH}_4$.

Simple trigonometry allows us to relate the values of $\boldsymbol{MH}_i$ with $d_D(j=0)$:

$$d_D(0)=[(h_1+h_4)\tau-h_0]$$

where $h_i=\boldsymbol{MH}_i.\ \boldsymbol{\nu}_i$.

We also have

$$d_Q(0)=[-h_0-(h_2+h_3)\tau^{-1}]$$
$$d'_D(0)=[h_0-(h_1+h_4)\tau]=-d_D(0)$$
$$d'_Q(0)=[+h_0+(h_2+h_3)\tau^{-1}]=-d_Q(0).$$

More generally, considering the triangles based on the $j$th set, we have

$$d_D(j)=-d'_D(j)=((h_{j+1}+j_{j-1})\tau-h_j) \tag{4.4a}$$
$$d_Q(j)=-d'_Q(j)=(-h_j-(h_{j-2}+h_{j+2})\tau^{-2}). \tag{4.4b}$$

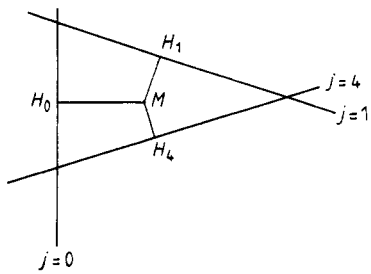


**Figure 15.** A triangle along the $j=0$ set.

Consider now the excitation

$$\delta\boldsymbol{\gamma}'_{\perp} = \delta\gamma'\boldsymbol{u}_3 = \delta\gamma'\sqrt{2/5}\left(1, -\frac{\tau}{2}, \frac{1}{2\tau'}, \frac{1}{2\tau'}, -\frac{\tau}{2}\right). \tag{4.5}$$

For a given mesh, this excitation will change $h_i$ onto

$$h_i^* = h_i + \delta\gamma_i. \tag{4.6}$$

Hence $d_D(0)$ will be transformed into $d_D^*(0)$. Using (4.4*a*) we have

$$\begin{aligned} d_D^*(0) &= (h_1^* + h_4^*)\tau - h_0^* \\ &= d_D(0) - \delta\gamma'\sqrt{2/5}(\tau+2) \\ &= d_D(0) - \delta\gamma'\sqrt{2}\tau. \end{aligned}$$

Let us call $\bar{d}_D(0) = +\delta\gamma'\sqrt{2}\tau$. $\bar{d}_D(0)$ is an important quantity in the following sense: the hexagons associated with each line of the $j=0$ set for which $0 < d_D(0) < \bar{d}_D(0) = \delta\gamma'\sqrt{2}\tau$ will be flipped by the excitation $\delta\boldsymbol{\gamma}'_{\perp}$, as depicted in figure 13. We also have

$$\begin{aligned} d_Q^*(0) &= d_Q(0) - \delta\gamma'\sqrt{2/5}(3-\tau) \\ &= d_Q(0) - \delta\gamma'\sqrt{2}/\tau \end{aligned}$$

and $\bar{d}_Q(0) = \delta\gamma'\sqrt{2}/\tau$. The lines for which $0 < d_Q(0) < \bar{d}_Q(0)$ will also be affected by the excitations in a similar way. The values of $d'_D$ and of $d'_Q$ will be increased by the excitation $\delta\boldsymbol{\gamma} = \delta\gamma'\boldsymbol{u}_3$, and the hexagons in the corresponding lines will not be shifted.

Table 2 summarises our results for the above excitations. For a given excitation and a given set $j$, it gives the value of $\bar{d}_D(j)$ and $\bar{d}_Q(j)$.

The excitation $\delta\boldsymbol{\gamma}'_{\perp} = \delta\gamma'\boldsymbol{u}_3$ given by (4.5) is invariant under reflection about the $\boldsymbol{\nu}_0$ direction. Under such a reflection the set $j=1$ is transformed into the set $j=4$, where $\bar{d}_D(1) = \bar{d}_D(4)$ and $\bar{d}_Q(1) = \bar{d}_Q(4)$. The same argument shows that $\bar{d}_D(2) = \bar{d}_D(3)$ and $\bar{d}_Q(2) = \bar{d}_Q(3)$.

The excitation

$$\delta\boldsymbol{\gamma}''_{\perp} = \delta\gamma''\boldsymbol{U}_4 = \delta\gamma''\left(0, \frac{1}{\tau}\sin\frac{2\pi}{5}, -\sin\frac{2\pi}{5}, \sin\frac{2\pi}{5}, -\frac{1}{\tau}\sin\frac{2\pi}{5}\right) \tag{4.7}$$

**Table 2**

| Excitation | | | |
|---|---|---|---|
| $\delta\boldsymbol{\gamma}'_{\perp} = \delta\gamma'\boldsymbol{u}_3$ | Set $j=0$<br>$\bar{d}_D^{(0)} = \sigma\gamma'\sqrt{2}\tau$<br>$\bar{d}_Q(0) = \delta\gamma'\dfrac{\sqrt{2}}{\tau}$ | Set $j=1$<br>$\bar{d}'_D(1) = \delta\gamma'\sqrt{2/5}\,\dfrac{3\tau+1}{2}$<br>$\bar{d}'_Q(1) = \delta\gamma'\sqrt{2/5}\,\dfrac{3\tau+1}{2\tau^2}$ | Set $j=2$<br>$\bar{d}(2) = \delta\gamma'\dfrac{\sqrt{2}}{2}$<br>$\bar{d}_Q(2) = \delta\gamma'\dfrac{\sqrt{2}}{2\tau^2}$ |
| $\delta\boldsymbol{\gamma}''_{\perp} = \delta\gamma''\boldsymbol{u}_4$ | Set $j=0$<br>$\bar{d}_D(0)$ unchanged<br>$\bar{d}_Q(0)$ unchanged | Set $j=1$<br>$\bar{d}_D(1) = \delta\gamma''\sqrt{2}$<br>$\bar{d}_Q(1) = \delta\gamma''\dfrac{\sqrt{2}}{\tau^2}$ | Set $j=2$<br>$\bar{d}'_D(2) = \delta\gamma''\sqrt{2}\tau$<br>$\bar{d}'_Q(2) = \delta\gamma''\dfrac{\sqrt{2}}{\tau}$ |
| $\delta\boldsymbol{\gamma}'''_D = \delta\gamma'''\boldsymbol{u}_0$ | Every set $j$<br>$\bar{d}'_D(j) = \delta\gamma'''$<br>$\bar{d}_Q(j) = \delta\gamma'''$ | | |

is transformed into $-\delta\boldsymbol{\gamma}''_\perp$ by reflection about the $\boldsymbol{\nu}_0$ direction. Hence, we have $\bar{d}_D(1) = \bar{d}'_D(4)$ and $\bar{d}_Q(1) = \bar{d}'_Q(4)$. Also $\bar{d}_D(2) = \bar{d}'_D(3)$ and $\bar{d}_Q(2) = \bar{d}'_D(3)$.

Finally the excitation $\boldsymbol{\delta\gamma}'''_D = \delta\gamma'''\boldsymbol{u}_0$ is invariant under a fivefold rotation; hence we have the same values of $\bar{d}_D(j)$ and $\bar{d}_Q(j)$ for every $j$.

Figure 16($a$) shows the various configurations of duals to hexagons in the pentagrid that are shifted from right to left (or vice versa) under the excitation $\delta\gamma'_\perp = \delta\gamma'\boldsymbol{u}_3$. The arrows indicate the direction in which the lines are displaced. Figure 16($b$) is the analogue of figure 16($a$) for $\delta\boldsymbol{\gamma}''_\perp = \delta\gamma''\boldsymbol{u}_4$. Figure 17 describes the excitation $\delta\gamma'''_D = \delta\gamma'''\boldsymbol{u}_0$.

An intriguing question is the following. Starting from a perfect PT defined by the set $(\gamma)_{i=0,\ldots,4}$, we introduce an excitation $\delta\boldsymbol{\gamma}$. Is it possible to distinguish between $\delta\boldsymbol{\gamma} \in P_\perp$ (i.e. a phason excitation) and $\delta\boldsymbol{\gamma} \in D$ (i.e. a structural transformation) knowing only the position of the modified strips in the tiling? To show that the answer is affirmative we proceed as follows.

We denote the height of triangles based on the zeroth line of the set $j = 0$ by $d^0_D(0)$. Similarly $d_D$ for the $i$th line is denoted $d^i_D(0)$. We have

$$0 < d^i_D(0) = m\tau - n + d^0_D(0) < \tau$$

$$0 < m - n\tau^{-1} + d^0_D(0)\tau^{-1} < 1$$

$$m = \lceil n\tau^{-1} - d^0_D(0)\tau^{-1} \rceil$$

and

$$d^i_D(0) = \left\lceil \frac{1}{\tau}\left(n - d^0_D(0)\right) \right\rceil \tau - n + d^0_D(0).$$

The lines of the set $j = 0$, which will be affected by the excitation $\delta\boldsymbol{\gamma} = \delta\gamma'\boldsymbol{u}_3$ are those for which

$$0 < d^i_D(0) < \delta\gamma'\sqrt{2} = d^i_D(0)$$

or

$$0 < m\tau - n + d^0_D(0) < \delta\gamma'\sqrt{2}$$

$$\left| m\tau - n + d^0_D(0) - \frac{\delta\gamma'\sqrt{2}}{2} \right| < \frac{\delta\gamma'\sqrt{2}}{2}.$$

And we have to solve the equation of the appendix with $x = d^0_D(0) - (\delta\gamma'\sqrt{2}/2)$ and $\omega = \delta\gamma'\sqrt{2}$. The result is the following: for $\tau^{-p} < \omega < \tau^{-p+1}$, the values of $n$ are $n = \{f_{p+1}, f_{p+2}, f_{p+3}\}$. This means that in the set $j = 0$, the distance between affected strips is equal to one of the above values of $n$. In the set $j = 1$, we have

$$0 < d'_D(1) < \delta\gamma'\sqrt{2/5}\,\frac{3\tau + 1}{2} = \bar{d}'_D(1) \tag{4.8}$$

which will generally give three (incommensurate) distances different from these that appear in the $j = 0$ set. Similarly for the $j = 2$ set

$$0 < d_D(2) < \delta\gamma'\sqrt{2} = \bar{d}_D(2) \tag{4.9}$$

which will give rise to three distances, different from the former.

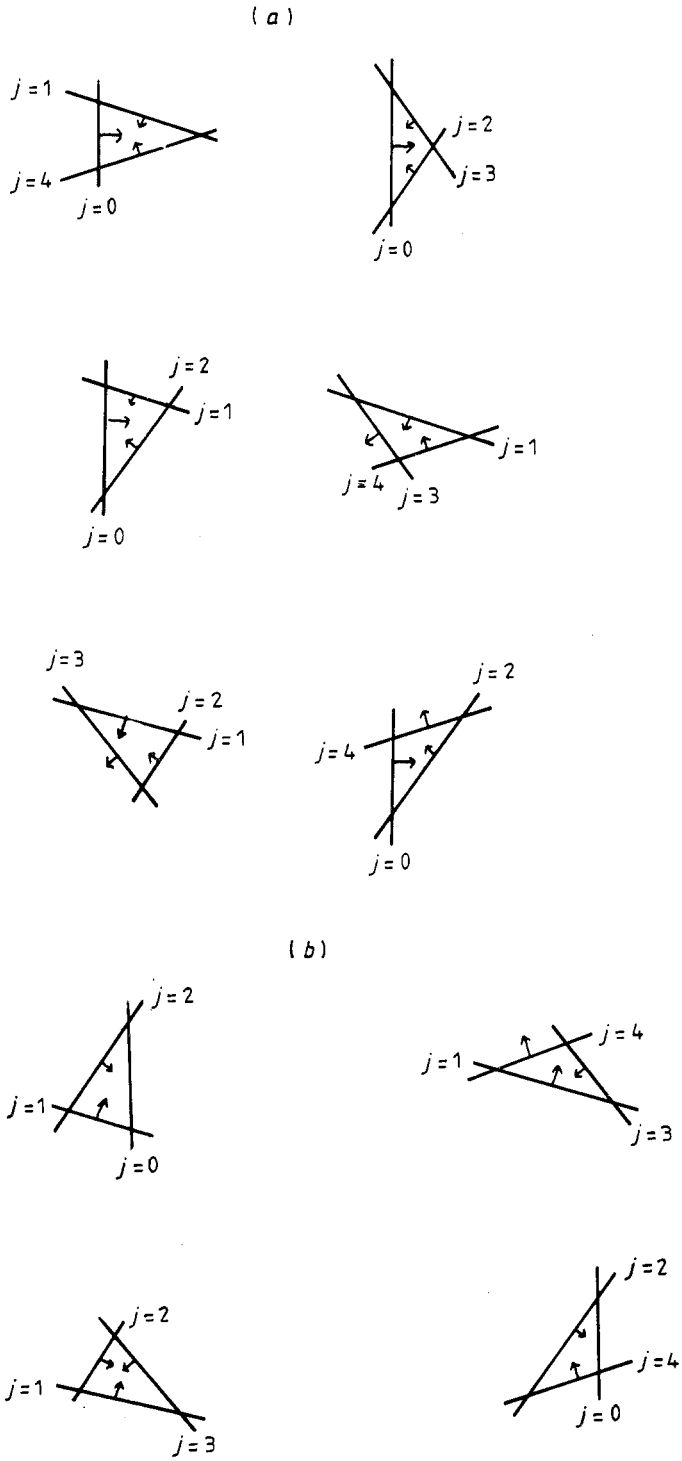


**Figure 16.** (*a*) Configurations of the pentagrid that are flipped under the excitations $\delta\gamma'_{\perp}$. The arrows indicate the directions in which the lines are moved. (*b*) The same as figure 16(*a*) for $\delta\gamma'''_{\perp}$.

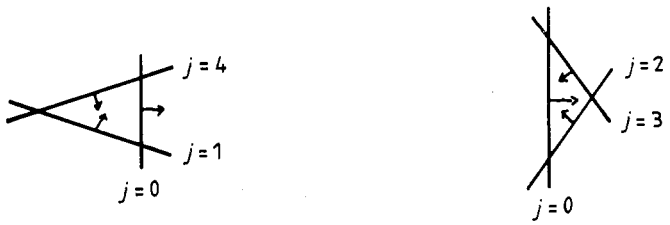


**Figure 17.** The same as figure 16(*a*) for $\delta\gamma_D'''$.

If we now consider an excitation $\delta\gamma = \delta\gamma \boldsymbol{u}_0$, lines of the sets $j = 0, \ldots, 4$ will be modified provided that

$$0 < d_D' < \delta\gamma = \bar{d}_D'.$$

This relation gives also rise to three distances. Since we have the same relation for all the sets of the tiling, the three distances will be the same for all the sets. Moreover in each set the three distances will appear with the same frequencies.

Figures 18(*a*) and 18(*b*) show a tiling with the excitation $\delta\gamma_\perp'' = 0.1\boldsymbol{u}_3$ and $\delta\gamma_\perp'' = 0.1\boldsymbol{u}_4$; while figure 19 depicts the excitation $\delta\gamma_D''' = 0.1\boldsymbol{u}_0$.

We have thus devised a method to distinguish between a phason excitation and a structural transformation. In a phason excitation, the modified lines in each set appear in three distances, which are different for each set. In a structural transformation, there are also three distances, which are the same for all sets.

## 5. Summary and discussion

We have considered here strips made of tiles adjacent along two parallel edges. We have shown that there are two types of strips. The first type consists of one-sided configurations (left-sided or right-sided): these configurations (worms) are separated by decagons. The second type consists of hybrids of both left-sided and right-sided configurations. The left-sided configurations are separated from the right-sided ones by interpenetrating decagons.

We have studied the statistics of the worms and found that their length (in terms of the numbers of hexagons they are made of) can assume only the values $L_n = f_n - 2$, $n \in \mathbb{N}$ ($f_n$ being a Fibonacci number). The density of worms of length $L$, $C(L)$, satisfies $C(L_n) \sim 1/L_n$. Worms terminate on decagons. There are several types of decagons, shown in figure 8(*c–e*). The statistics of the decagons are calculated in § 3.

We have also introduced perturbations in the underlying pentagrid and analysed the statistics of the distances among worm lines which are affected by those perturbations. We have shown that a phason excitation is located along worms such that the distance between two affected worms belonging to the set $j$ may take only three possible values. These values are different for each set. A structural transformation excitation is also located along worms. The distance between two perturbed worms takes only three values, which are the same for each set. As we have remarked in the introduction, the relation of this analysis to real physical systems is not obvious. Should we associate the generation of mismatches with activation energy? Is their propagation (along worm and through decagons) described in terms of a thermal hopping process? What are

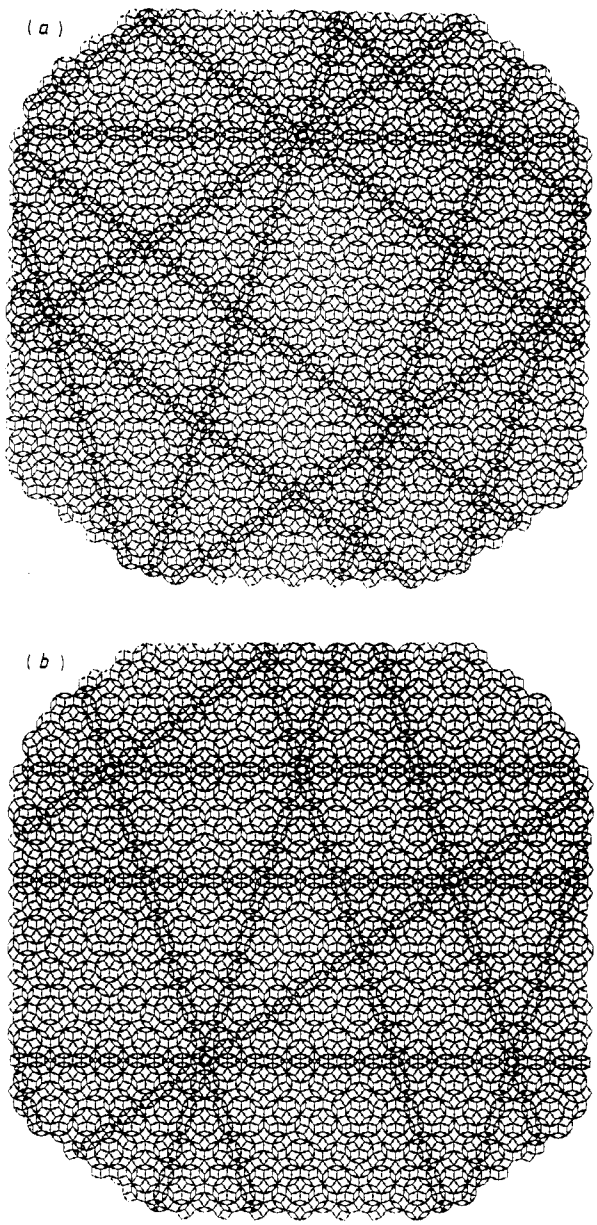


**Figure 18.** Positions of shifted hexagons under the excitations (*a*) $\delta\gamma'_{\perp}$, (*b*) $\delta\gamma''_{\perp}$.

the characteristic energies involved? Also, is this picture affected by the presence of other (topological) defects? All these questions await their answer in the future.

## Acknowledgments

YG is a Bat Sheva de Rothschild fellow. AP is grateful to the Weizmann Institute for hospitality and financial support.

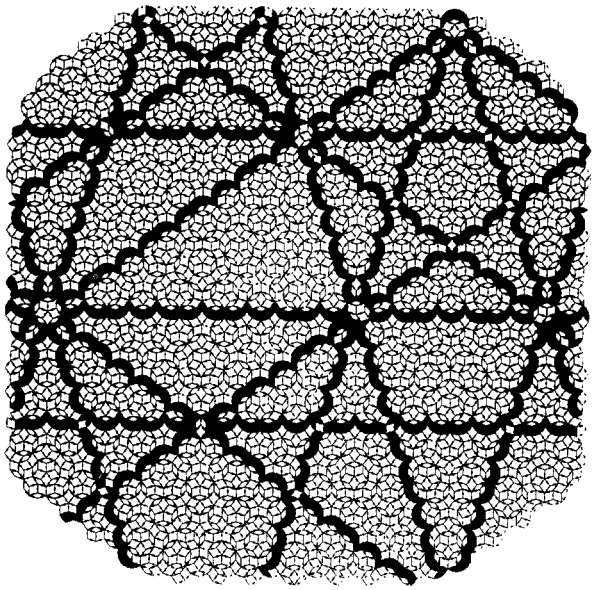

**Figure 19.** Positions of the new tiles that appear under the excitation $\delta\gamma''_D$.

## Appendix

The aim of this appendix is to solve equation (3.1*b*) which is of the form

$$|x+\tau m-n|<\omega/2 \tag{A1}$$

where $n$ and $m$ are integers and $x$ and $\omega$ are two real numbers such that

$$0<\omega<1 \qquad \text{and} \qquad |x|<\omega/2. \tag{A2}$$

The second condition of equation (A2) means that for $m$ and $n$ equal to zero, equation (A1) is obeyed, and the problem is to find the pair $(n, m)$ such that equation (A1) is obeyed ($n+m$ being the minimal positive number).

We interpret equation (A1) as follows. Consider a circle of unit perimeter centred at $D$ and a 'window' of length $\omega = OA'$ (see figure 20), measured along the perimeter, starting at O. Start from point S at a distance $x+\omega/2$ from O along the perimeter. Since equation (A2) is obeyed, S is always within the window. We then move in steps of length $\tau$ along the circle and reach point $F$ (not shown in figure 17). Equation

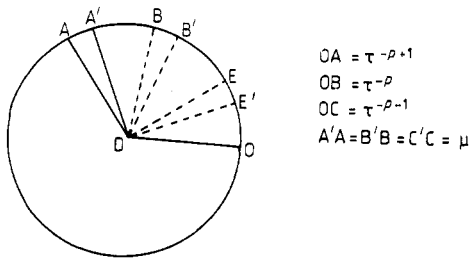


**Figure 20.** 'Windows' on the unit circle.

(A1) states that F must be within the window. Suppose that

$$\tau^{-p} < \omega < \tau^{-p+1} \tag{A3}$$

which we write as

$$\omega = \tau^{-p+1} - \mu. \tag{A4}$$

Let us also define A, B, C, B′ and C′ on the unit circle, such that

$$OA = \tau^{-p+1} \qquad OB = \tau^{-p} \qquad OC = \tau^{-p-1} \qquad B'B = C'C = A'A = \mu.$$

We now note that for S within the segment OC′, we end up back in the window after $f_p$ steps of length $\tau$; for S within CA′ we need $f_{p+1}$ $\tau$-steps and for S within CC′, we need $f_{p-2}$ $\tau$-steps, where $f_p$ are the Fibonacci numbers defined in Coxeter (1969). When $\mu = 0$, i.e. $\omega = \tau^{-p+1}$, the only $\tau$-step 'periodicities' are $f_p$ and $f_{p+1}$, corresponding respectively to the windows OC and CA.

Let us first consider the case $\omega = \tau^{-p+1}$ corresponding to the window OA. We have the following relation (Coxeter, 1969):

$$\tau f_p = (-\tau)^{-p} + f_{p+1}. \tag{A5}$$

When $p$ is odd, this reads

$$\tau f_p = \tau^{-p} + f_{p+1} \tag{A6a}$$

$$\tau f_p + \tau^{-p-1} = \tau^{-p+1} + f_{p+1}. \tag{A6b}$$

These equations can be interpreted as follows: from (A6$a$) we see that choosing a starting point at 0, after $f_p$ $\tau$-steps, the final point is B ($OB = \tau^{-p}$); from (A6$b$) we see that choosing C as our starting point, after $f_p$ $\tau$-steps, we end up at A. This means that the interval OC is mapped onto the interval BA. If we replace $p$ by $p+1$ in equation (A5) we have

$$\tau f_{p+1} + \tau^{-p-1} = f_{p+2} \tag{A7a}$$

$$\tau f_{p+1} + \tau^{-p+1} = f_{p+2} + \tau^{-p} \tag{A7b}$$

from (A7$a$) we see that choosing C as our starting point ($OC = \tau^{-p-1}$), after $f_{p+1}$ $\tau$-steps, the final point 0 is reached; similarly from (A7$b$) after $f_{p+1}$ $\tau$-steps take as from A to B ($OB = \tau^{-p}$). Hence the interval CA is mapped onto the interval OB. Similar analysis holds for $p$ odd. Hence we see that for $\omega = \tau^{-p+1}$, the pairs $(n, m) = (f_{p+1}, f_p)$ and $(f_{p+2}, f_{p+1})$ are solutions of equation (A1). There are no solutions with $(m+n)$ smaller (that would correspond to an approximant to the golden ratio, better than its contonuous fraction expansion).

When $\mu \neq 0$, the demonstration of A1 goes as follows: let us consider the points A′, B′ and C′ ($p$ is taken to be even). Then the interval OC′ is transformed by $f_p$ $\tau$-steps into BA′ and the interval CA′ is transformed by $f_{p+1}$ $\tau$-steps into OB′. We are left with the interval C′C, which is transformed by $f_p$ $\tau$-steps into A′A and after $f_{p+1}$ $\tau$-steps into B′B. Hence points in the interval C′C require, $f_p + f_{p+1} = f_{p+2}$ $\tau$-steps. The solutions of equation (A1) are the pairs $(n, m) = \{f_{P+1}, f_p\}$, $\{f_{p+2}, f_{p+1}\}$ and $\{f_{p+3}, f_{p+2}\}$.

The relative weight of a given worm of length $m+n+2$ is obtained by noting that it is proportional to the range of values of $x$ (equation A1), for which this worm exists.

## References

Alexander S 1986 *J. Phys. Colloq.* C3 **47** 143
Bak P 1985 *Phys. Rev. Lett.* **54** 1517
—— 1986 *Phys. Rev.* B **32** 5764
Biham O, Mukamel D and Shtrikman S 1986 *Phys. Rev. Lett.* **56** 2191
Bohsung J and Trebin H-R 1987 *Phys. Rev. Lett.* **58** 1204
de Bruijn N G 1981a *Proc. Konink. Nederlandse Akad.* A **84** 39
—— 1981b *Proc. Konink. Nederlandse Akad.* A **84** 53
Coxeter H S M 1969 *Introduction to Geometry* (New York: Wiley)
Duneau M and Katz A 1985 *Phys. Rev. Lett.* **54** 2688
Entin-Wohlamn O, Kléman M and Pavlovitch A 1988 *J. Physique* **49** 587
Frenkel D M, Henley C L and Siggia E D 1986 *Phys. Rev.* B **34** 3649
Gardner M 1977 *Sci. Am.* **236** 110
Gefen Y, Kléman M, Pavlovitch A and Peyrière J 1989 *J. Physique* in press
Gratias D and Michel L 1986 *J. Physique* C3 **47** 1988
Grünbaum B and Sheppard G C 1987 *Tilings and Patterns* (San Francisco: Freemen)
Henley C L 1987 *Comment. Condensed Matter Phys.* B **13** 59
Katz A and Duneau M 1986 *J. Physique* **47** 181
Kléman M, Gefen Y and Pavolovitch A 1986 *Europhys. Lett.* **1** 61
Kramer P and Néri R 1984 *Acta Crystallogr.* A **40** 580
Levine O, Lubensky T C, Ostlund S, Ramaswamy S, Steinhardt P J and Toner J 1985 *Phys. Rev. Lett.* **54** 1520
Niven I 1956 *Irrational Numbers* (New York: Wiley)
Pavlovitch A and Kléman M 1987 *J. Phys. A: Math. Gen.* **20** 687
Penrose R 1974 *Bull. Inst. Math. Appl.* **10** no. 7/8
—— 1979 *Mathematical Intelligencer* **2** 32
Peyrière J 1986 *J. Phys. COlloq.* C3 **47** 41
Sadoc J F and Mosseri R 1984 *J. Non-Crystal Solids* **61/62** 487
Socolar J E S, Lubensky T C and Steinhardt P J 1986 *Phys. Rev.* B **34** 3345